Accepted Manuscript

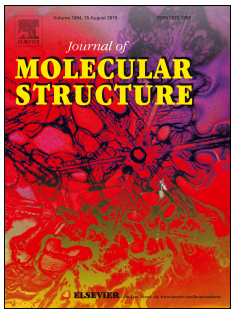

Spectral characterization, computed frequencies analysis and electronic structure calculations on (1E)-*N*-hydroxy-3-(1*H*-imidazole-1-yl)-1-phenylpropan-1-imine: An oxime-bearing precursor to potential antifungal agents

Reem I. Al-Wabli, Munusamy Govindarajan, Maha S. Almutairi, Mohamed I. Attia

PII: S0022-2860(18)30582-9

DOI: 10.1016/j.molstruc.2018.05.022

Reference: MOLSTR 25194

To appear in: *Journal of Molecular Structure*

Received Date: 6 March 2018

Revised Date: 23 April 2018

Accepted Date: 7 May 2018

Please cite this article as: R.I. Al-Wabli, M. Govindarajan, M.S. Almutairi, M.I. Attia, Spectral characterization, computed frequencies analysis and electronic structure calculations on (1E)-*N*-hydroxy-3-(1*H*-imidazole-1-yl)-1-phenylpropan-1-imine: An oxime-bearing precursor to potential antifungal agents, *Journal of Molecular Structure* (2018), doi: 10.1016/j.molstruc.2018.05.022.

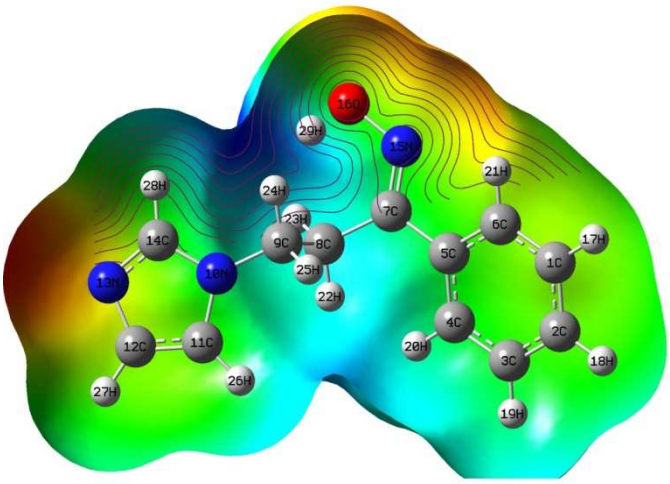

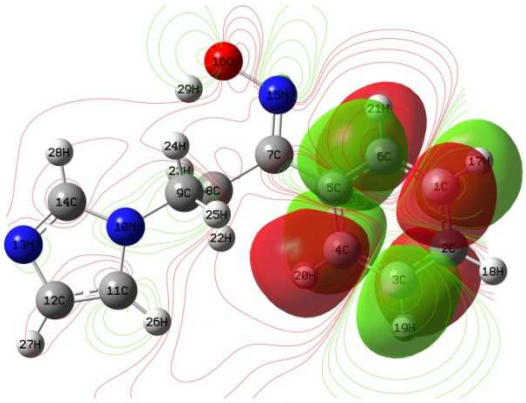

LUMO + 1 = -0.6615

Spectral characterization, computed frequencies analysis and electronic structure calculations on (1*E*)-*N*-hydroxy-3-(1*H*-imidazol-1-yl)-1-phenylpropan-1-imine: An oxime-bearing precursor to potential antifungal agents

Reem I. Al-Wabli[a], Munusamy Govindarajan[b,c], Maha S. Almutairi[a] and Mohamed I. Attia[a,d]*

[a]Department of Pharmaceutical Chemistry, College of Pharmacy, King Saud University, P.O. Box 2457, Riyadh 11451, Saudi Arabia
[b]Department of Physics, Avvaiyar Government College for Women (AGCW), Karaikal, Puducherry 609602, India
[c]Department of Physics, Arignar Anna Government Arts and Science College for Women (AAGASC), Karaikal, Puducherry 609602, India
[d]Medicinal and Pharmaceutical Chemistry Department, Pharmaceutical and Drug Industries Research Division, National Research Centre, Dokki, Giza 12622, Egypt

Keywords: Imidazole; FT-IR; FT-Raman; HOMO-LUMO; DFT/B3LYP and HF.

Abstract:

(1*E*)-*N*-Hydroxy-3-(1*H*-imidazol-1-yl)-1-phenylpropan-1-imine (H3IPI) is a precursor to potential antifungal agents and was subjected to experimental and simulated spectroscopic (UV, FT-IR, FT-Raman as well as ^{1}H and ^{13}C NMR) characterization. Density functional theory, Hartfock fundamental wavenumbers and intensity of the modes are interpreted with the aid of structure optimizations and normal force field computations. The complete wavenumbers assignments of H3IPI were made on the basis of potential energy distribution of each vibrational mode. The electronic and excited state properties have been determined by time dependent-density functional theory method. The responsiveness parameters as chemical potential, global hardness, and electrophilicity index have also been calculated. The scaled B3LYP/6-311++G(d,p) calculations showed better coincidence with the experimental findings of H3IPI over the other computation method. Molecular electrostatic potential and thermodynamic properties of the title compound were also investigated. In addition, Mulliken and natural charges distribution, non-linear optics properties as well as natural bond orbital analysis of the title molecule were calculated and interpreted. Theoretical calculations of the NMR chemical shifts of H3IPI were carried out through GIAO method at B3LYP/6-311++G(d,p) level and the results were compared with the experimental values.

1. Introduction

The incidence of systemic fungal infections (IFIs) has significantly escalated over the past two decades giving rise to high rates of morbidity and mortality particularly in immunocompromised individuals such as patients taking anticancer chemotherapy or undergoing organ transplants and patients with AIDS [1-3]. Polyenes [4], echinocandins [5], antimetabolites [6] and azoles [7] are the major categories of the currently available antifungal drugs in clinic in which azoles constitute a milestone in the antifungal therapy.

Since the appearance of imidazole-bearing antifungal agents in late 1980s, they are widely applied as efficient antifungal drugs but resistance development limits their current therapeutic use in clinic [8]. In addition, the antifungal agents manifested certain toxicity to human systems due to similarity between the human and fungi molecular processes [9]. Therefore, the development of new azole-bearing antifungal agents remains an open interesting research area to acquire safer antifungal candidates capable of countering resistance of the serious fungal infections

Most of the currently available antifungal agents feature a two carbon bridge between aromatic and azole pharmacophore moieties, while a limited number of the available antifungal agents have a three carbon spacer between the aromatic and the azole pharmacophore fragments [10-13]. Moreover, some potent azole-bearing antifungal agents were prepared from starting materials having oxime functionality [14].

Amalgamation of two or more biologically active pharmacophore fragments in one molecular hybrid chemical entity became a popular approach in medicinal chemistry to get modified scaffolds endowed with much improved and amazing biological properties [15].

The aforementioned premises persuaded us to synthesis the title molecule as an amalgamated molecular hybrid bearing oxime functionality as well as the aromatic and imidazole pharmacophore moieties with a three carbon chain spacer. The title molecule compromises the required structural features to be functionalized in the synthesis of new imidazole-bearing antifungal agents. Vibrational analysis and spectral (FT-IR, FT-Raman, UV, ^{1}H and ^{13}C NMR) characterization of the title compound was carried out in the current study with the aid of *ab initio* Hartree-Fock (HF) and DFT computational approaches. Furthermore, Molecular electrostatic potential (MEP), natural bond orbital (NBO) analysis**,** nonlinear optic (NLO) activity and HOMO-LUMO analysis were also computed for the title molecule. We believe that the results of the current investigations might support the development of improved potent and safer antifungal agents.

2. Experimental details

2.1. General

The title molecule H3IPI was synthesized as previously reported [13]. The FT-IR spectrum H3IPI has been recorded in Perkin-Elmer 180 spectrometer in the range of 4000–400 cm^{-1}. The spectral resolution is ± 2 cm^{-1}. The FT-Raman spectrum of H3IPI was also recorded using the same instrument with FRA 106 Raman module equipped with Nd: YAG laser source operating in the region 100-4000 cm^{-1} at 1.064 μm line widths with 200 mW powers. The spectra were recorded with scanning speed of 30 cm^{-1}/min and spectral width of 2 cm^{-1}. The frequencies of all sharp bands are accurate within ± 1 cm^{-1}. Bruker NMR spectrometer was used to record NMR spectra of the title compound in deuterated chloroform ($CDCl_3$) at 500 MHz for ^{1}H and 125.76 MHz for ^{13}C at the Research Center, College of Pharmacy, King Saud University, Saudi Arabia.

2.2. Synthesis

The commercially available acetophenone (2.4 g, 20 mmol) was dissolved in absolute ethanol (35 mL). Paraformaldehyde (0.81 g, 9 mmol), dimethylamine hydrochloride (2.2 g, 27 mmol) and a catalytic amount of concentrated hydrochloric acid (0.1 mL) were added to the ethanolic reaction solution. The reaction mixture was stirred and refluxed for two hours, cooled and acetone (30 mL) was added. Mannich base hydrochloride (**1**) was precipitated, collected by filtration and dried. Imidazole (1.4 g, 20 mmol) was added to the aqueous solution of compound **1** (2.1 g, 10 mmol) in water (10 mL). The reaction mixture was stirred and refluxed for five hours and cooled. Compound **2** was precipitated and collected by filtration to give the ketone **2** in 77% yield which were pure enough to be used in the next step. The ketone **2** (2.00 g, 10 mmol), hydroxylamine hydrochloride (1.39 g, 20 mmol), and KOH (1.12 g, 20 mmol) in ethanol (10 mL) were heated to reflux under stirring for 18 h. The reaction mixture was cooled to room temperature and the insolubles were filtered off. The filtrate was concentrated under vacuum and the residue was poured onto ice-cold water (15 mL). The precipitated solid was filtered, dried, and recrystallized from ethanol to give 1.51 g (70%) of the oxime **3** as colorless crystals mp 427-429 K (lit. 428-430 K [13]). ^{1}H-NMR ($CDCl_3$): δ 7.58 (s, 1H, -N-C*H*=N-), 7.29–7.49 (m 5H, Ar-H), 7.07 (s, 1H, -N-CH=C*H*-N=), 6.96 (s, 1H, -N-C*H*=CH-N=), 4.28 (t, *J* = 7.1 Hz, 2H, -CH_2-CH_2-N), 3.31 (t, *J* = 7.1 Hz, 2H, -CH_2-CH_2-N).

2.3. Quantum chemical calculations

The entire quantum chemical calculations have been performed at DFT (B3LYP) and *ab initio* HF methods with 6-311++G(d,p) basis set using the Gaussian 09 program [16]. The optimized structural parameters have been evaluated for the calculations of wavenumbers at different level of theories. At the minimum geometry for the H3IPI molecule no negative wavenumber modes were obtained, therefore a true minimum was found on the potential energy of the molecule. Consequently, the computed wavenumbers, reduced masses, force constants, infrared intensities, Raman activities, Raman intensities, and depolarization ratios were obtained. The computed harmonic frequencies were scaled down to improve the computed values. Therefore, the calculated wavenumbers at HF level were scaled by 0.905 [17] and the range of wavenumbers were scaled by 0.958 and 0.983 above and below 1700 cm^{-1}, respectively, for B3LYP/6-311++G(d,p) [18, 19]. After using this scaling factor, the deviation from the experimental values is less than 10 cm^{-1} with a few exceptions. The appointments of the

calculated normal modes have been made on the basis of the corresponding PEDs. The PEDs were calculated from the quantum chemically computed wavenumbers using VEDA program [20]. GaussView program [21] has been considered to get visual animation and also for the verification of the normal modes assignment.

The electronic absorption spectra for optimized H3IPI molecule calculated with time dependent density functional theory (TD-DFT) at B3LYP/6-311++G (d,p) level. The molecular electrostatic potential of H3IPI was evaluated to investigate its reactive sites. Furthermore, in order to show the nonlinear optic (NLO) activity of the H3IPI molecule, the dipole moment, linear polarizability and first hyperpolarizability were obtained from its molecular polarizabilities based on theoretical calculations. Moreover, the changes in the thermodynamic functions (the heat capacity, entropy and enthalpy) of H3IPI were investigated at different temperatures.

2.4. Prediction of Raman intensities

The calculated Raman activities (S_{Ra}) with Gaussian 03 program were converted to the relative Raman intensities (I_{Ra}) using the following relationship derived from the intensity theory of Raman scattering [22]:

$$I_i = \frac{f\left(\nu_0 - \nu_i\right)^4 S_i}{\nu_i\left[1 - \exp\left(-hc\nu_i / kT\right)\right]} \qquad (1)$$

where; ν_0 is the laser exciting wavenumber in cm^{-1} (ν_0 = 9398.5 cm^{-1}, which corresponds to the wavelength of 1064 nm of a Nd:YAG laser), ν_i the vibrational wavenumber of the i^{th} normal mode (cm^{-1}), while S_i is the Raman scattering activity of the normal mode ν_I, f is a constant equal to 10^{-12} and was suitably chosen with common normalization factor for all peak intensities. *h, k, c* and *T* are Planck constant, Boltzmann constant, speed of light and temperature in Kelvin, respectively.

3. Results and discussion

3.1. Synthesis

The title molecule **3** was prepared in a three step reaction sequence as presented in Scheme 1 using the commercially available acetophenone as a starting material according to the reported procedure [13]. The spectral data of the synthesized H3IPI are in accordance with the recorded ones.

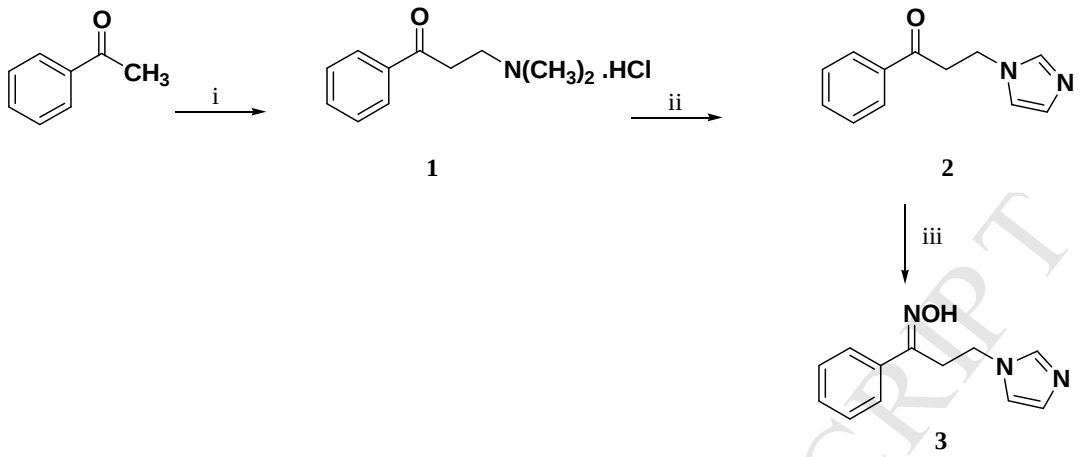

Reagents and conditions: i) $HN(CH_3)_2$.HCl, $(CH_2O)_n$, conc. HCl, ethanol, reflux, 2 h; ii) Imidazole, water, reflux, 5 h; iii) H_2NOH.HCl, KOH, ethanol, reflux, 18 h.

Scheme 1: Synthesis of the title compound **3**.

3.2. Molecular geometry

The optimized DFT geometries of the H3IPI molecule by B3LYP/6-311++G(d,p) and its molecular structure with atoms numbering are shown in Figure 1. The internal coordinates described the position of atoms in terms of distances, angles and dihedral angles with respect to an origin atom. By allowing the relaxation of all parameters, the calculations were made up of scan coordinate 1 (C6-C5-C7-C8) and scan coordinate 2 (C5-C7-C8-C9) by rotating angle from 0 to 360°. It met the optimized geometries, which correspond to the true energy minima, as revealed by the lack of imaginary frequencies in the vibrational mode calculations. The symmetry coordinates were constructed using a set of internal coordinates. A full set of 81 standard internal coordinates for the H3IPI molecule are presented in Figure 2. The molecules were linked together by a strong intermolecular O16· · ·N13 bond with 0.900 Å bond length.

The optimized geometry of H3IPI was calculated by PM3 and was re-calculated by B3LYP and HF methods. The bond lengths evaluated by B3LYP method were longer than that obtained by HF and PM3 methods. The H3IPI molecule has one O-H, one O-N, five C-N, ten C-C and twelve C-H bond lengths. The optimized parameters of H3IPI by B3LYP and HF methods at 6-311++G(d,p) level as well as the experimental values [23] are indicated in Table 1. The B3LYP/6-311++G(d,p) method overestimates bond lengths, particularly the C-H bond lengths. The average aromatic C–H bond lengths in the H3IPI molecule were calculated as 1.083 Å using B3LYP/6-311++G(d,p) method and 1.093 Å in the propylidene side chain. The aromatic C–H bond lengths are shorter in both HF method and experimental. The shortest C11–H26 bond

length is presented as 1.069 Å in the HF/6-311++G (d,p) method. On the other hand, the C-C bond distances of H3IPI were found to have higher values in case of B3LYP calculations with respect to HF computations. The longest C-C bond length was calculated for C8-C9 using B3LYP /6-311++G(d,p) to be 1.546 Å, while the shortest C-C bond length was found in the C11-C12 (1.371 Å) using the same computation method. The shortest experimental C-N bond was found to be 1.285 Å for N15-C7 bond, while the O16-H29 bond is the shortest (0.900 Å) experimental O-H vibration. The calculated O–N bond lengths were found to be 1.381 and 1.372 Å using B3LYP and HF methods, respectively, at 6-311++G(d,p) level of theory.

Table 1: Optimized structural parameters (bond lengths (Å), bond angles and dihedral angles (°)) of H3IPI calculated by HF and B3LYP methods with 6-311++G(d, p) level.

Bond	HF	B3LYP	Exp.[a]	Bond	HF	B3LYP	Exp.[a]
Bond lengths (Å)							
O16-N15	1.372	1.381	1.403	C3-C4	1.386	1.393	1.388
O16-H29	0.943	0.970	0.900	C3-H19	1.076	1.084	0.950
N15-C7	1.260	1.286	1.285	C4-C5	1.390	1.402	1.400
N10-C9	1.447	1.454	1.466	C4-H20	1.075	1.083	0.950
N10-C14	1.350	1.370	1.350	C5-C7	1.463	1.489	1.485
N10-C11	1.373	1.382	1.374	C7-C8	1.515	1.516	1.511
N13-C12	1.369	1.375	1.378	C8-C9	1.535	1.546	1.534
N13-C14	1.291	1.311	1.319	C8-H22	1.082	1.089	0.990
C6-C1	1.381	1.388	1.391	C8-H23	1.082	1.097	0.990
C6-C5	1.395	1.405	1.398	C9-H24	1.083	1.092	0.990
C6-H21	1.073	1.082	0.950	C9-H25	1.080	1.092	0.990
C1-C2	1.388	1.395	1.389	C14-H28	1.072	1.081	0.950
C1-H17	1.076	1.084	0.950	C11-C12	1.351	1.371	1.359
C2-C3	1.382	1.391	1.389	C11-H26	1.069	1.078	0.950
C2-H18	1.076	1.084	0.950	C12-H27	1.070	1.079	0.950
Bond angles (°)							
C7-N15-O16	113.19	112.66	111.57	C5-C4-H20	120.56	120.62	119.6
C14-N10-C11	105.94	105.26	106.95	C6-C5-C4	118.57	118..30	118.63
C14-N13-C12	105.05	105.18	105.09	C6-C5-C7	120.34	119.84	120.40
C1-C6-C5	120.60	120.73	120.45	C4-C5-C7	121.09	121.86	120.90
C1-C6-H21	120.18	120.57	119.8	C5-C7-C8	120.89	120.14	120.70
C6-C1-H17	119.63	119.56	119.8	C7-C8-C9	112.10	110.22	114.95
C2-C1-C6	120.34	120.41	120.27	C7-C8-H22	108.35	110.55	108.5
C2-C1-H17	120.03	120.02	119.9	C9-C8-H22	108.86	109.00	108.5
C5-C6-H21	119.22	118.61	119.9	C7-C8-H23	110.24	111.84	108.5
C3-C2-C1	119.57	119.46	119.75	C9-C8-H23	109.73	109.30	108.5

C3-C2-H18	120.22	120.25	120.1	N10-C9-C8	112.11	112.76	114.23
C1-C2-H18	120.21	120.29	120.1	N10-C9-H24	107.71	107.92	108.7
C4-C3-C2	120.12	120.26	120.14	C8-C9-H24	110.71	110.21	108.7
C4-C3-H19	119.64	119.51	119.9	N10-C9-H25	108.89	108.97	108.7
C2-C3-H19	120.23	120.18	119.9	C8-C9-H25	109.78	109.66	108.7
C3-C4-C5	120.80	120.83	120.72	C11-C12-N13	110.33	110.60	110.14
C3-C4-H20	118.64	118.53	119.6	C12-C11-N10	105.78	105.64	105.94
Dihedral angles (°)							
C5-C6-C1-C2	0.0662	-0.085	0.5	N15-C7-C8-C9	77.72	-83.378	66.1
C6-C1-C2-C3	0.1261	0.1987	1.1	C5-C7-C8-C9	-102.51	-91.935	-114.85
C1-C2-C3-C4	-0.1301	-0.1224	-1.3	C14-N10-C11-C12	-0.1929	-0.2625	-0.1
C3-C4-C5-C6	-0.504	-0.069	-0.1	C9-N10-C11-C12	177.57	176.98	176.87
C1-C6-C5-C4	-0.2458	-0.019	-1.9	N13-C12-C11-N10	0.1027	0.146	0.1
C1-C6-C5-C7	179.49	179.95	175.03	C9-N10-C14-N13	-177.60	-177.03	-176.95
C3-C4-C5-C6	0.504	0.049	1.7				
C3-C4-C5-C7	-178.93	-179.48	-175.24				
O16-N15-C7-C5	-179.27	-176.83	-178.52				
O16-N15-C7-C8	0.8549	-1.33	0.6				
C6-C5-C7-C8	-156.49	-151.84	-145.59				
C6-C5-C7-N15	23.62	23.85	31.3				
C6-C5-C7-C8	-156.49	-151.84	35.2				

[a]Atoms numbering as indicated in Figure 1.

The experimental values of the angles are C1–C6–C5 (120.45°), C2–C1–C6 (120.27°), C3–C2–C1 (119.75°), C4–C3–C2 (120.14°), C3–C4–C5 (120.72°) and C6-C5-C4 (118.63°) in which they are closer to the values calculated by the HF method than that calculated by B3LYP method. The smallest experimental dihedral angle was manifested for C14-N10-C11-C12 to be -0.1° in the H3IPI molecule. The calculated bond angles of the title molecule suggest a distortion in its aromatic ring which might be due to steric and electronic factors. The graphical expression between the experimental and calculated bond lengths and bond angles are represented in Figure S1.

Bond length

$$\mu cal = 0.34267 + 0.75043\mu \exp \qquad (R^2 = 0.98064) HF \qquad (2)$$

$$\mu cal = 0.35321 + 0.75123\mu \exp \qquad (R^2 = 0.98631) B3LYP \qquad (3)$$

Bond angle

$$\phi cal = 2.99553 + 0.97437\phi \exp \qquad (R^2 = 0.97165) HF \qquad (4)$$

$$\phi cal = 4.94878 + 0.95750\phi \exp \qquad (R^2 = 0.94707) B3LYP \qquad (5)$$

3.3. Mulliken and natural charges distribution

The wavenumbers of the molecule is directly related to its Mulliken charges, and quantifies how the electronic behavior alters under atomic displacement. Therefore, it is directly related to the chemical bonds present in the molecule. Major contribution of Mulliken charges involves dipole moment, polarizability, electronic structure of the molecule. The Mulliken and natural charge distribution of the H3IPI molecule are calculated on HF and B3LYP levels at gaseous phase and the values are given in Table 2, while their graphs are presented in Figure 3. The Mulliken charges distribution on the title compound showed that all carbon atoms attached with hydrogen atoms are negatively charged expect C7, which manifested about 0.275722 and 0.119624 in HF and B3LYP, respectively. The natural charges distribution also exhibited the same trend. Moreover, the Mulliken and natural charges distribution on N10 and N13 possesses more negative values than on N15. In both Mulliken and natural charges using HF/6-311++G(d,p), the H29 atom showed the highest positive value (0.366224 and 0.43835, respectively) due to its attachment to the electronegative oxygen atom. The natural charges of all hydrogen atoms are positive with higher values than Mulliken charges.

Table 2: Muilliken and natural charges distribution using B3LYP and HF methods at 311++G(d,p) level.

Atom	Muilliken charges distribution		Natural charges distribution	
	B3LYP	HF	B3LYP	HF
C1	-0.093994	-0.152501	-0.19308	-0.18190
C2	-0.079357	-0.142897	-0.19771	-0.18732
C3	-0.097622	-0.151905	-0.19293	-0.18164
C4	-0.072321	-0.154646	-0.18681	-0.17478
C5	-0.100630	-0.038884	-0.08195	-0.09191
C6	-0.027714	-0.121181	-0.18301	-0.16974
C7	0.119624	0.275722	0.17243	0.21458
C8	-0.272107	-0.266487	-0.43674	-0.38944
C9	-0.052193	-0.003425	-0.16634	-0.09397
N10	-0.313809	-0.623881	-0.43523	-0.52231
C11	-0.009793	0.046267	-0.07053	-0.03810
C12	-0.057939	0.000234	-0.06196	-0.03532
N13	-0.301359	-0.544873	-0.49821	-0.55605
C14	0.155669	0.339315	0.20112	0.29621
N15	-0.116732	-0.212585	-0.09361	-0.09796
O16	-0.275306	-0.514838	-0.50814	-0.55960
H17	0.101489	0.155698	0.20793	0.19697
H18	0.099648	0.155858	0.20771	0.19682
H19	0.097239	0.155654	0.20759	0.19660

H20	0.091674	0.147615	0.20871	0.19763
H21	0.110464	0.179439	0.21366	0.20341
H22	0.142537	0.178108	0.23188	0.20790
H23	0.120154	0.146813	0.18916	0.16761
H24	0.136121	0.140600	0.21136	0.18661
H25	0.150257	0.173627	0.22023	0.19775
H26	0.105427	0.170017	0.20943	0.19973
H27	0.102980	0.145350	0.20355	0.19391
H28	0.108512	0.151563	0.19597	0.18595
H29	0.229082	0.366224	0.42554	0.43835

3.4. Thermodynamic properties

The global minimum energies obtained for structure optimization of H3IPI are *ca* -704.68625 a.u. and -700.1511 a.u. using B3LYP and HF methods, respectively, with 6-311++G(d,p) basis set without any symmetric constrains. The mean energy difference between the two computational methods is *ca* 4 a.u. only. The thermal energies are also in the same trend with global minimum energies of the H3IPI molecule. The rotational constants are falling in values from HF to B3LYP method and the entropy values are more eminent in the B3LYP/6-311++G(d,p) method. The biggest value of zero point vibrational energy of the H3IPI molecule is 146.95501 (Kcal/Mol) obtained at B3LP/6-311++G(d,p). The charge distribution of a molecule counts on the dipole moment in the three dimensions and the direction of the dipole moment in the H3IPI molecule shows the focus on the positive and negative charges.

The thermodynamic parameters, heat capacity (C), entropy (S) and enthalpy changes (ΔH) of H3IPI by DFT/B3LYP method at different temperatures and 1.00 atm pressure were obtained from the theoretical harmonic frequencies are listed in Table 3. These thermodynamic functions are changing with temperature ranging from 100 to 1000 K due to the fact that the molecular vibrational wavenumbers increase with temperature [24]. Correlation equations between heat capacities, entropies, enthalpy changes and temperatures were fitted by quadratic polynomial formulas, and the corresponding fitting factors (R^2) for these thermodynamic properties are 0.999967, 0.9999 and 0.9999, respectively. The corresponding fitting equations are as follows and their correlation graphics are illustrated in Figure 4.

$$C = 1.07395 + 0.21048\,T - 8.53284 \times 10^{-5}\,T^2 \qquad (R^2 = 0.99967) \qquad (6)$$

$$S = 61.35032 + 0.21623\,T - 4.40243 \times 10^{-5}\,T^2 \qquad (R^2 = 0.99995) \qquad (7)$$

$$\Delta H = -1.2347 + 0.01048\,T + 7.14841 \times 10^{-5}\,T^2 \qquad (R^2 = 0.99906) \qquad (8)$$

The thermodynamic data furnished helpful information for further study on the H3IPI molecule. The thermodynamic data can be used to compute the early thermodynamic energies according to the relationships of thermodynamic functions and calculate directions of chemical reactions according to the second law of thermodynamics in the thermo chemical field [25].

Table 3: Thermodynamic properties at different temperatures of H3IPI at the B3LYP/6-311++G(d,p) level.

Temperature	Heat capacity	Entropy	Enthalpy changes
100	21.654	82.808	1.347
200	39.292	102.236	3.213
300	56.846	122.740	7.826
400	70.560	140.396	14.160
500	85.316	158.777	21.613
600	97.643	175.196	30.649
700	106.452	191.087	41.105
800	114.339	206.222	54.629
900	121.550	220.289	65.976
1000	126.197	233.530	79.926

3.5. Ultraviolet spectra analysis and Frontier molecular orbitals (FMOs)

The highest occupied molecular orbitals (HOMOs) and the lowest-lying unoccupied molecular orbitals (LUMOs) are named as frontier molecular orbitals (FMOs). The FMOs play a key role in the optical and electric properties, as well as in UV–Vis spectra of the molecules [26]. Gauss-Sum 2.2 program [27] was used to calculate group contributions to the molecular orbital (HOMO and LUMO) of the H3IPI molecule as shown in Figure 5. The HOMO represents the power to give an electron, while LUMO as an electron acceptor represents the ability to obtain an electron. The gap between HOMO and LUMO energies determines the kinetic stability, chemical responsiveness, optical polarization and chemical hardness–softness of the molecule.

In order to measure the energetic behavior of H3IPI, the calculations were carried out in

acetonitrile, chloroform, toluene and ethanol. According to the probe of FMO energy levels of the H3IPI molecule, the corresponding electronic shifts between HOMO and LUMO as well as between HOMO-1 and LUMO+1 can be found. The energies of the four important molecular orbitals (the highest occupied MO's (HOMO and HOMO−1) and the lowest unoccupied MO's (LUMO and LUMO+1)) of H3IPI were calculated using B3LYP/6-311++G(d,p) and presented in Table 4. The calculated HOMO energy value of H3IPI is -6.1819, -6.1328, -6.0816 and -6.1784 eV in acetonitrile, chloroform, toluene and ethanol, while its LUMO is -1.1767, -1.1829, -1.1946 and -1.1770 eV, respectively. The value of the energy gap between the HOMO and LUMO is -5.0052, -4.9499, -4.8870 and -5.0014 eV in acetonitrile, chloroform, toluene and ethanol, respectively.

Table 4: Calculated energy values of H3IPI in acetonitrile, chloroform, toluene and ethanol using B3LYP/6-311++G(d,p).

Parameter	**Acetonitrile**	**Chloroform**	**Toluene**	**Ethanol**
E_{total} (Hartree)	-704.529	-704.525	-704.522	-704.529
E_{HOMO} (eV)	-6.1819	-6.1328	-6.0816	-6.1784
E_{LUMO} (eV)	-1.1767	-1.1829	-1.1946	-1.1770
$\Delta E_{HOMO\text{-}LUMO\ gap}$ (eV)	-5.0052	-4.9499	-4.8870	-5.0014
$E_{HOMO\text{-}1}$ (eV)	-6.3253	-6.3286	-6.3392	-6.3253
E_{LUMO+1} (eV)	-0.1653	-0.1735	-0.1873	-0.1659
$\Delta E_{HOMO\text{-}1\text{-}LUMO+1\ gap}$ (eV)	-6.1600	-6.1551	-6.1518	-6.1594
Electronegativity χ (eV)	2.5026	2.4749	2.4435	2.5007
Chemical hardness η (eV)	3.6793	3.6579	3.6381	3.6777
Electrophilicity index ψ (eV)	0.8511	0.8372	0.8205	0.8501
Dipole moment (Debye)	4.8683	4.7206	4.5647	4.8584

The energy break of HOMO–LUMO explains the charge shift interaction within H3IPI, which influences its biological activity. 3D plots of the HOMO and LUMO orbitals of H3IPI computed at the B3LYP/6-311++G(d,p) level are illustrated in Figure 5. The red color indicates positive sites, while the green color indicates the negative ones. It is authorizing that, while the HOMO is placed on the whole H3IPI molecule especially localized on the imidazole ring and CNO group, the LUMO is placed on the benzene ring CNO and CH_2 groups. The HOMO→LUMO transition implies an electron density transfer from oxygen atom.

The value of electronegativity, chemical hardness and electrophilicity index of H3IPI in acetonitrile are 2.5026, 3.6793 and 0.8511 eV, respectively, which are higher than the values

calculated in chloroform, toluene and ethanol. The dipole moment in a molecule is another important electronic property. For example, the bigger the dipole moment, the stronger will be the intermolecular interactions. The calculated dipole moment values for the title molecule are also given in Table 4. Based on the predicted dipole moment values, it was found that, the highest value (4.8683 Debye) was obtained in acetonitrile.

Ultraviolet spectra analyses of H3IPI have been investigated in acetonitrile, chloroform, toluene and ethanol by theoretical calculations. On the basis of fully optimized ground-state structure, TD-DFT/B3LYP/6-311++G(d,p) calculations have been used to determine the low-lying excited states of H3IPI. The theoretical electronic excitation energies, oscillator strengths and absorption wavelengths of H3IPI are listed in Table 5 and its theoretical as well as experimental UV spectra are presented in Figure S2. Calculations of the molecular orbital geometry of H3IPI showed that its absorption maxima corresponds to the electron transition between frontier orbitals such as translation from HOMO to LUMO. As can be seen from Table 5, the calculated absorption maxima values have been found to be 272.75, 252.55, 251.91, 237.83 and 220.49 nm for acetonitrile, 276.36, 252.75, 252.64, 238.28 and 222.81 nm for chloroform, 280.44, 253.13, 252.66, 238.82 and 225.49 nm for toluene and 272.99, 252.57, 252.05, 237.87 and 220.63 nm for ethanol at DFT/B3LYP/6-311++G(d,p) level.

Table 5: Theoretical electronic absorption spectra of E3IYLPI absorption wavelengths λ (nm), excitation energies E (eV) and oscillator strengths (*f*)) using TD-DFT/B3LYP/6-311++G(d,p) method in different solvents.

Solvent	**E (eV)**	**λ (nm)**	**(*f*)**
	4.5457eV	272.75nm	f=0.0058
	4.9094 eV	252.55nm	f=0.0374
Acetonitrile	4.9217eV	251.91 nm	f=0.3606
	5.2131eV	237.83nm	f=0.0050
	5.6232eV	220.49nm	f=0.0240
	4.4864 eV	276.36 nm	f=0.0057
	4.9054 eV	252.75 nm	f=0.2418
Chloroform	4.9075 eV	252.64 nm	f=0.1729
	5.2033eV	238.28 nm	f=0.0064
	5.5645 eV	222.81nm	f=0.0045
	4.4211 eV	280.44 nm	f=0.0055
	4.8980 eV	253.13 nm	f=0.2892
Toluene	4.9071 eV	252.66 nm	f=0.1326
	5.1916 eV	238.82 nm	f=0.0086

	5.4984 eV	225.49 nm	f=0.0032
	4.5418 eV	272.99 nm	f=0.0058
	4.9090 eV	252.57 nm	f=0.0444
Ethanol	4.9190 eV	252.05 nm	f=0.3565
	5.2123 eV	237.87 nm	f=0.0051
	5.6195 eV	220.63 nm	f=0.0178

3.6. Molecular electrostatic potential

A 3D plot of molecular electrostatic potential (MEP) map of H3IPI is illustrated in Figure 6. This MEP is a plot of electrostatic potential mapped onto the constant electron density surface. The importance of MEP lies in the fact that the molecular shape as well as the positive, negative and neutral electrostatic potential regions of the molecule can be displayed in one figure in terms of color grading which is very useful to generate a relationship between molecular structure and its physiochemical properties [28, 29]. In addition, the MEP is a useful property to study the reactivity of the molecule as an approaching electrophile will be attracted to the negative regions and the nucleophile will attack the positive regions in the molecule. In the majority of MEPs, the maximum negative regions are indicated as red colors, while the positive regions are indicated as blue colors. The negative electrostatic potential is preferred on nitrogen occupied regions, while the positive electrostatic potential is preferred on $(CH_2)_2$ occupied regions.

The different values of the electrostatic potential at the surface of the H3IPI molecule are represented by different colors. The potential increases in the order red < orange < yellow < green < blue. The color code of the H3IPI map is in the range between -0.05929 a.u. (deepest red) to 0.05929 a.u. (deep blue color). Where the blue color indicates the strongest attraction and the red color indicates the strongest repulsion. The electron density (ED) value of H3IPI was found to be within the range of -0.01766 to +0.01766 a.u. As can be seen from the MEP map of the title molecule, while regions having the negative potential are over the nitrogen and oxygen atoms, the regions having the positive potential are over all hydrogen atoms. The front and side views of ethylene group in H3IPI have a green color indicating neutral potential.

3.7. Non-Linear optics (NLO) properties

The first hyperpolarizability (β), dipole moment (μ) and polarizability (α) were calculated for H3IPI using HF/6-311++G(d,p) basis set on the basis of the finite-field approach. The complete equations for calculating the magnitude of total static dipole moment (μ), the mean

polarizability (α_0), the anisotropy of the polarizability ($\Delta\alpha$) and the mean first polarizability (β_0), using the *x*, *y*, *z* components from Gaussian 03W program output are as follows:

$$\alpha_{tot} = \frac{1}{3}\left(\alpha_{xx} + \alpha_{yy} + \alpha_{zz}\right) \qquad (9)$$

$$\Delta\alpha = \frac{1}{\sqrt{2}}\left[\left(\alpha_{xx} - \alpha_{yy}\right)^2 + \left(\alpha_{yy} - \alpha_{zz}\right)^2 + \left(\alpha_{zz} - \alpha_{xx}\right)^2 + 6\alpha_{xz}^2 + 6\alpha_{xy}^2 + 6\alpha_{yz}^2\right]^{\frac{1}{2}} \qquad (10)$$

$$\langle\beta\rangle = \left[\left(\beta_{xxx} + \beta_{xyy} + \beta_{xzz}\right)^2 + \left(\beta_{yyy} + \beta_{yzz} + \beta_{yxx}\right)^2 + \left(\beta_{zzz} + \beta_{zxx} + \beta_{zyy}\right)^2\right]^{\frac{1}{2}} \qquad (11)$$

The total dipole moment was calculated using the following equation:

$$\mu_{tot} = \left(\mu_x^2 + \mu_y^2 + \mu_z^2\right)^{\frac{1}{2}} \qquad (12)$$

The calculated parameters described above for the title compound were listed in Table 6. It is well known that the higher values of dipole moment, molecular polarizability, and hyperpolarizability result in more active NLO properties. The polarizabilities and hyperpolarizability are reported in atomic units (a.u.), the calculated values have been converted into electrostatic units (esu) (for α, 1 a.u. = 0.1482 x 10^{-24} esu and for β, 1 a.u. = 8.6393 x 10^{-33} esu). The calculated value of the total dipole moment (μ_{total}) of H3IPI was found to be 1.8915 Debye. The highest value of dipole moment was observed for component μ_z (0.0995 D). The calculated polarizability of H3IPI is 1363.48 x 10^{-33} esu. The magnitude of molecular hyperpolarizability (β) is an important key factor in the NLO system. The dipole moment and first hyperpolarizability of the title molecule are about 1.32 and 3.66 times greater than those of the standard NLO compound, urea (μ and β of urea are 1.3732 Debye and 372.8 x 10^{-33} esu obtained by HF/6-311++G(d,p) method).

Table 6: The electric dipole moment, polarizability and first hyperpolarizability of H3IPI.

Parameter	**a.u.**	**esu (×10^{-24})**	**Parameter**	**a.u.**	**esu (×10^{-33})**
α_{xx}	196.54	29.12781	β_{xxx}	10.816	93.44526
α_{xy}	12.86	1.90606	β_{xxy}	-25.345	-218.966
α_{yy}	170.51	25.2698	β_{xyy}	-49.569	-428.244
α_{xz}	3.02	0.448769	β_{yyy}	-134.145	-1161.25
α_{yz}	-1.64	-0.24436	β_{xxz}	12.1756	105.1887
α_{zz}	109.85	16.23113	β_{xyz}	-16.661	-143.947
α_{total}	128.221	19.002	β_{yyz}	-38.456	-332.238
μ_x	-1.5816		β_{xzz}	9.9800	86.22042
μ_y	-0.8939		β_{yzz}	-10.330	-89.2461

μ_z	0.995	β_{zzz}	9.0154	77.88726
μ_{total}	1.8915	β_0	157.823	1363.48

3.8. Natural bond orbital (NBO) analysis

Natural bond orbital (NBO) analysis has been expressed away to explain the delocalization of charges due to interactions among bonds, and also it provides a convenient basis for looking into conjugative interactions in molecular systems. The presence of electron donor orbitals and electron acceptor orbitals in the molecular system gives rise stabilization energy resulting from the second-order micro disturbance theory is reported [30]. The greater the stabilization energy value, the more intensive is the fundamental interaction between electron donors and electron acceptors, i.e. the more donating trend from electron donors to electron acceptors and the greater the extent of junction of the whole system. Delocalization of electrons concentration between occupied Lewis-type (bond or lone pair) NBO orbitals and formally unoccupied (anti bond or Rydberg) non-Lewis NBO orbitals is corresponding to the stabilizing donor–acceptor interaction. These interactions were observed in case of increasing the ED in C-C anti-bonding orbital that weakens the respective bonds. These intramolecular charge transfer ($\sigma\rightarrow\sigma^*$, $\pi\rightarrow\pi^*$) can induce large nonlinearity of the molecule.

The strong intramolecular hyperconjugation interactions of σ and π electrons of the C-C, C-H, C-N and N-C bonds to the anti C-C, C-H, C-N and N-C bonds lead to stabilization of some parts of the H3IPI molecule as evident from Table 7. NBO analysis has been performed on the title molecule at the B3LYP/6-311++G(d,p) level in order to elucidate its intramolecular hyperconjugation interactions, re-hybridization and delocalization of the electron density within the molecule. The interaction was formed by the orbital convergence between the bonding (C-C) and the anti-bond (C-C) orbital which results intramolecular charge transfer (ICT) causing stabilization of the system. These interactions were observed as an increase in the electron density in the C–C anti-bonding orbital that weakens the respective bonds. The solid intramolecular hyperconjugative interaction of the σ electrons of (C_1–C_2) distributed to σ^*(C_1–C_6, C_1–H_{17}, C_2–C_3, C_2–H_{18}, C_3–H_{19} and C_6–H_{21}) of the aromatic moiety of H3IPI. On the other hand, the π(C_1–C_6) in the aromatic ring conjugates to the anti-bonding orbital of π^*(C_2–C_3 and C_4–C_5) leading to strong delocalization of 0.28 kJ/mol. The π(C_2-C_3) is interacting with π^*(C_1-C_6 and C_4-C_5) with the energies 0.29 and 0.28 kcal/mol, respectively. The π(C_1–C_6) is contributing energy by 0.28 kcal/mol with π^*(C_2–C_3). In a reverse trend, the π(C_2–C_3) is contributing energy

by 0.29 kcal/mol with $\pi^*(C_1–C_6)$. Similarly, the $\sigma(C_7\text{-}N_{15})$ is acting with $\sigma^*(C_4–C_5, C_5–C_7, C_7–C_8$ and $O_{16}–H_{29})$ with energy values of 1.48, 1.37, 1.31 and 1.32 kcal/mol, respectively. The $\sigma(N_{10}\text{-}C_{11}$ and $N_{10}\text{-}C_{14})$ are acting with $\sigma^*(C_9–N_{10}$ and $N_{13}–C_{14})$ with values of 1.12, 1.36 and 1.14, 1.38 kcal/mol, respectively. The LP(1) of N_{15} and O_{16} are moving with $LP^*(1)(C_5\text{-}C_7)$ with values of 0.89 and 1.15 kcal/mol, respectively.

Table 7: Second order perturbation theory analysis of Fock matrix in NBO basis for H3IPI.

Donor (i)	Type of bond	Occupancy	Acceptor (j)	Type of bond	Occupancy	E2 (kJ.mol^{-1})[a]	E(j) −E(i) (a.u.)[b]	F(i, j) (a.u.)[c]
C1-C2	σ	1.97923	C1-C6	σ*	0.01587	3.07	1.28	0.056
			C1-H17	σ*	0.01468	1.09	1.14	0.031
			C2-C3	σ*	0.01686	2.96	1.27	0.055
			C2-H18	σ*	0.01457	1.10	1.14	0.032
			C3-H19	σ*	0.01440	2.52	1.14	0.048
			C6-H21	σ*	0.01457	2.39	1.16	0.047
C1-C6	σ	1.97801	C1-C2	σ*	0.01728	3.08	1.27	0.056
			C1-H17	σ*	0.01468	1.14	1.15	0.032
			C2-H18	σ*	0.01457	2.36	1.15	0.046
			C5-C6	σ*	0.02473	3.66	1.26	0.061
			C5-C7	σ*	0.03480	3.60	1.16	0.058
			C6-H21	σ*	0.01457	1.20	1.16	0.033
C1-C6	π	1.66685	C2-C3	π*	0.32273	20.72	0.28	0.068
			C 4-C5	π*	0.37586	20.10	0.28	0.068
C2-C3	σ	1.97907	C1-C2	σ*	0.01728	2.94	1.27	0.055
			C1-H17	σ*	0.01468	2.43	1.15	0.047
			C2-H18	σ*	0.01457	1.13	1.15	0.032
			C3-C4	σ*	0.01599	3.14	1.28	0.057
			C3-H19	σ*	0.01440	1.15	1.14	0.032
			C4-H20	σ*	0.01487	2.44	1.14	0.047
C2-C3	π	1.66136	C1-C6	π*	0.29363	19.09	0.29	0.067
			C4-C5	π*	0.37586	20.66	0.28	0.069
C4-C5	σ	1.97263	C3-C4	σ*	0.01599	3.44	1.27	0.059
			C3-H19	σ*	0.01440	2.12	1.14	0.044
			C4-H20	σ*	0.01487	1.30	1.14	0.034
			C5-C6	σ*	0.02473	4.33	1.25	0.066
			C5-C7	σ*	0.03480	2.81	1.15	0.051
			C6-H21	σ*	0.01457	2.26	1.15	0.046
			C7-N15	σ*	0.01864	1.46	1.28	0.039
C4-C5	π	1.65090	C1-C6	π*	0.29363	18.78	0.29	0.067
			C2-C3	π*	0.32273	19.89	0.29	0.068
			C7-N15	π*	0.17579	15.99	0.27	0.062
C5-C6	σ	1.97086	C1-C6	σ*	0.01587	3.25	1.27	0.058
			C1-H17	σ*	0.01468	2.22	1.13	0.045
			C4-C5	σ*	0.02436	4.42	1.25	0.066
			C4-H20	σ*	0.01487	2.67	1.13	0.049
			C5-C7	σ*	0.03480	2.95	1.14	0.052
			C6-H21	σ*	0.01457	1.19	1.15	0.033
			C7-C8	σ*	0.03423	2.42	1.08	0.046
C5-C7	σ	1.96109	C1-C6	σ*	0.01587	2.01	1.24	0.045
			C3-C4	σ*	0.01599	2.27	1.23	0.047
			C4-C5	σ*	0.02436	2.49	1.22	0.049

			C5-C6	σ*	0.02473	2.79	1.21	0.052
			C7-C8	σ*	0.03423	1.31	1.05	0.033
			C7-N15	σ*	0.01864	2.35	1.24	0.048
			N15-O16	σ*	0.02145	5.23	0.87	0.060
C7-C8	σ	1.97455	C5-C6	σ*	0.02473	2.29	1.20	0.047
			C5-C7	σ*	0.03480	2.00	1.10	0.042
			C7-N15	σ*	0.01864	1.80	1.23	0.042
			C8-C9	σ*	0.02218	0.71	0.99	0.024
			C8-H22	σ*	0.01514	0.59	1.05	0.022
			C8-H23	σ*	0.01317	0.60	1.05	0.022
			C9-N10	σ*	0.02891	2.33	0.98	0.043
			N15-O16	σ*	0.02145	0.64	0.86	0.021
C7-N15	σ	1.98928	C4-C5	σ*	0.37586	1.77	1.48	0.046
			C5-C7	σ*	0.03480	2.27	1.37	0.050
			C7-C8	σ*	0.03423	2.03	1.31	0.046
			O16-H29	σ*	0.00375	0.51	1.32	0.023
C8-C9	σ	1.96602	C5-C7	σ*	0.03480	1.04	1.07	0.030
			C7-C8	σ*	0.03423	0.97	1.02	0.028
			C7-N15	σ*	0.01864	3.25	0.64	0.042
			C8-H22	σ*	0.01514	0.59	1.03	0.022
			N10-C11	σ*	0.02391	0.53	1.07	0.021
			N10-C14	σ*	0.04246	1.28	1.08	0.033
C9-N10	σ	1.98650	C7-C8	σ*	0.03423	1.29	1.16	0.035
			N10-C11	σ*	0.01514	1.47	1.22	0.038
			N10-C14	σ*	0.04246	1.39	1.23	0.037
			C11-C12	σ*	0.01880	0.75	1.36	0.029
			N13-C14	σ*	0.00912	0.86	1.34	0.030
N10-C11	σ	1.98151	C9-N10	σ*	0.02891	1.70	1.12	0.039
			N10-C14	σ*	0.04246	2.17	1.25	0.047
			C11-C12	σ*	0.01880	1.25	1.38	0.037
			C12-N13	σ*	0.01133	0.66	1.29	0.026
			C12-H27	σ*	0.01804	3.03	1.24	0.055
			N13-C14	σ*	0.00912	0.62	1.36	0.026
			C14-H28	σ*	0.02233	2.66	1.21	0.051
N10-C14	σ	1.98610	C9-N10	σ*	0.02891	1.86	1.14	0.041
			C9-H24	σ*	0.01345	0.52	1.19	0.022
			N10-C11	σ*	0.02391	2.12	1.25	0.046
			C11-H26	σ*	0.01266	2.67	1.24	0.051
			N13-C14	σ*	0.00912	0.67	1.38	0.027
C11-C12	σ	1.98384	C9-N10	σ*	0.02891	5.86	1.04	0.070
			N10-C11	σ*	0.02391	0.98	1.15	0.030
			C11-H26	σ*	0.01266	2.06	1.14	0.043
			C12-N13	σ*	0.01133	0.59	1.20	0.024
			C12-H27	σ*	0.01804	1.51	1.16	0.037
C12-N13	σ	1.97842	N10-C11	σ*	0.02391	0.96	1.20	0.030
			N10-C14	σ*	0.04246	1.19	1.21	0.034
			C11-C12	σ*	0.01880	1.20	1.34	0.036
			C11-H26	σ*	0.01266	3.41	1.18	0.057
			N13-C14	σ*	0.00912	0.62	1.32	0.026
			C14-H28	σ*	0.02233	5.15	1.17	0.069
N13-C14	σ	1.98504	C9-N10	σ*	0.02891	3.80	1.15	0.059
			N10-C14	σ*	0.04246	0.83	1.28	0.029
			C12-N13	σ*	0.01133	0.61	1.32	0.025
			C12-H27	σ*	0.01804	3.23	1.27	0.057
			C14-H28	σ*	0.02233	1.13	1.24	0.033
N10	LP(1)	1.55892	C7-C8	LP*(1)	0.03423	0.61	0.65	0.020

			C8-C9	LP*(1)	0.02218	5.89	0.60	0.060
			C9-H24	LP*(1)	0.01345	0.61	0.65	0.020
			C9-H25	LP*(1)	0.01740	3.07	0.66	0.045
N13	LP(1)	1.92363	C9-N10	LP*(1)	0.02891	0.59	0.68	0.018
			N10-C14	LP*(1)	0.04246	8.34	0.81	0.074
			C11-C12	LP*(1)	0.01880	5.50	0.94	0.065
			C12-H27	LP*(1)	0.01804	2.19	0.80	0.038
			C14-H28	LP*(1)	0.02233	2.23	0.77	0.037
N15	LP(1)	1.95757	C5-C7	LP*(1)	0.03480	0.63	0.89	0.021
			C7-C8	LP*(1)	0.03423	9.46	0.83	0.079
			O16-H29	LP*(1)	0.00375	0.75	0.84	0.023
O16	LP(1)	1.99274	C5-C7	LP*(1)	0.03480	0.63	1.15	0.024
			C8-H23	LP*(1)	0.01317	0.73	1.10	0.025

[a] E(2) means energy of hyper conjugative interactions; [b] Energy difference between donor and acceptor i. and j. NBO orbitals; [c] F(i, j) is the Fock matrix element between i .and j. NBO orbitals.

3.9. NMR spectra and calculations

The experimental and theoretical ^{1}H and ^{13}C NMR chemical shifts of H3IPI are described in ppm relative to TMS and the data are presented in Table 8 and their spectra are shown in Figures S4 and S5. Full geometry optimization of H3IPI was firstly carried out at the gradient corrected density functional level of theory using the hybrid B3LYP method based on Becke's three parameters functional of DFT. Thereafter, gauge-including atomic orbital (GIAO) ^{1}H and ^{13}C chemical shift calculations of H3IPI was performed by the same method using 6-311G++(d,p) basis set IEFPCM/$CDCl_3$ solution.

Table 8: Experimental and theoretical probable ^{13}C and ^{1}H NMR chemical shifts of the H3IPI molecule.

Atom*	Experimental	Theoretical	Atom*	Experimental	Theoretical
C1	128.9	132.7	H17	7.3	6.8
C2	135.1	133.3	H18	7.4	7.1
C3	128.9	131.5	H19	7.3	7.0
C4	128.8	128.5	H20	7.5	7.1
C5	137.0	137.6	H21	7.5	7.1
C6	128.8	131.4	H22	3.3	3.3
C7	155.4	160.7	H23	3.3	2.1
C8	28.3	32.4	H24	4.3	3.5
C9	41.8	44.0	H25	4.3	4.1
C11	119.1	120.6	H26	6.9	6.6
C12	126.1	128.3	H27	7.1	6.6
C14	139.5	139.8	H28	7.6	7.7

* Atoms positions are numbered as in Figure 1.

The aromatic ring carbon atoms committed signals in the covered areas of the ^{13}C spectrum with chemical shift values from 128.5-137.6 ppm, while their corresponding experimental values were observed in the range of 128.8-137.0 ppm. The highest experimental chemical shift values were noticed for C7 and C14 carbon atoms at 155.4 and 139.5 ppm, respectively. On the other hand, the lowest chemical shift values were observed for C8 and C9 carbon atoms at 28.3 and 41.8 ppm, respectively.

The aromatic ring hydrogens of H3IPI were accumulated in the range of 6.8-7.1 ppm (B3LYP) and are experimentally observed in the range of 7.3-7.5 ppm. The performance of the B3LYP method with respect to the prediction of the NMR chemical shifts within the H3IPI molecule is quite close to the experimental values.

3.10. Vibrational analysis

The maximum number of potentially active observable fundamentals of a non-linear molecule containing N atoms is equal to (3N-6), apart from three translational and three rotational degrees of freedom [31]. The H3IPI molecule is planar with 29 atoms and 81 normal modes of vibrations and it is considered under C_s point group symmetry. The fundamental modes are distributed in the C_s symmetry species as: $\Gamma_{vib} = 55A' + 26A''$. Here A′ represents symmetric planer and A″ asymmetric non-planer vibrations. All vibrations are active in both Raman and infrared absorptions. The detailed vibrational assignments of the experimental wavenumbers are based on normal mode analyses of the title compound. The scaled wavenumbers following B3LYP/6-311++G(d,p) method were found to be closer to the experimental data than the results obtained using HF method. The observed and simulated FT-IR and FT-Raman spectra of H3IPI are shown in Figures 7 and 8, respectively. The observed and scaled theoretical frequencies using HF/6-311++G(d,p) and DFT/B3LYP/6-311++G(d,p) basis sets with their potential energy distributions (PEDs) are listed in Table 9.

Table 9: Detailed assignments of theoretical and experimental wavenumbers of H3IPI along with their potential energy distributions (PEDs) assignments.

Serial number	FT-IR	FT-Raman	HF/6-311++G(d,p) scaled	B3LYP/6-311++G(d,p)				
				I_{IR}	S_{Raman}	unscaled	scaled	assignments
1	3238		3805	147.03	163.60	3835	3674	γOH
2	3148	3148	3126	1.28	94.08	3265	3128	γCH
3	3116		3101	4.35	107.87	3238	3102	γCH
4			3090	3.12	37.32	3231	3095	γCH
5		3063	3078	3.47	110.43	3206	3072	γCH

6			3061	11.84	227.40	3193	3059	γCH
7	3049		3052	25.20	58.43	3185	3051	γCH
8			3041	5.05	136.20	3174	3041	γCH
9		3022	3031	1.08	41.80	3166	3033	γCH
10	3002		2997	9.16	1.97	3125	2994	γCH
11		2974	2979	0.08	52.75	3105	2974	γCH
12		2859	2944	20.03	4.39	3075	2946	γCH
13			2933	5.29	132.42	3063	2934	γCH
14	1644		1749	4.42	94.29	1677	1648	βOH
15	1600	1623	1640	0.56	259.14	1639	1611	γCC
16	1574	1597	1611	1.99	18.56	1612	1585	γCC
17		1515	1566	28.56	5.44	1535	1509	γCC
18			1531	22.61	12.68	1528	1502	γCC
19	1507	1497	1514	21.35	21.90	1527	1501	γCC
20	1474	1476	1486	10.86	4.30	1503	1477	γCN
21	1455		1475	50.91	16.48	1488	1462	γCN
22	1441		1456	3.99	4.35	1473	1448	γCN
23		1400	1408	3.58	16.62	1413	1389	γCN
24			1399	18.95	79.12	1402	1378	γCN
25	1368	1369	1390	24.21	40.51	1393	1369	γNO
26	1351	1344	1386	1.99	32.33	1382	1359	γCC
27			1335	2.61	2.77	1355	1332	γCC
28	1313		1309	12.30	4.08	1332	1310	γCC
29	1296		1300	0.60	2.38	1317	1295	γCC
30			1287	51.37	13.23	1310	1287	βCH
31	1277	1279	1260	20.25	20.40	1301	1279	βCH
32	1255		1247	65.56	34.73	1279	1258	βCH
33		1230	1214	40.69	5.92	1258	1237	φOH
34	1184	1185	1180	2.89	4.62	1207	1187	βCH
35		1164	1160	0.34	6.07	1185	1165	βCH
36		1158	1112	1.68	23.96	1181	1161	βCH
37	1105		1108	18.83	6.82	1139	1120	βCH
38		1102	1086	3.78	1.24	1109	1090	βCN
39	1079		1077	18.18	17.36	1094	1075	βCN
40			1076	27.00	8.66	1086	1067	βCN
41	1040		1050	10.38	39.10	1048	1030	βCN
42	1024	1027	1024	10.44	3.21	1046	1028	βNO
43			1024	49.65	1.10	1029	1012	βCN
44			1016	7.81	21.37	1023	1006	βCN
45	997	998	1011	1.28	56.12	1015	998	βCH
46			1004	0.71	0.82	1010	992	βCH
47	972		988	0.42	0.25	991	974	βCH
48		924	959	123.71	2.36	942	926	βCH
49	924		951	12.30	0.50	937	921	βCH
50	893		908	8.09	1.38	917	902	βCCC
51	852	854	903	2.42	1.75	870	855	βCCC
52			876	0.27	1.31	855	841	βCCC
53	823		867	6.63	2.80	846	832	βNO
54	780		831	30.74	0.55	810	796	βCCC

55		768	780	24.36	2.29	785	771	βCCC
56	758		768	19.92	0.52	772	759	φCH
57			761	31.14	1.62	732	720	φCH
58			711	14.45	1.70	730	717	φCH
59	699		700	39.73	0.26	705	693	φCH
60	672	671	661	14.41	0.10	673	661	φCH
61		654	645	26.79	3.58	658	646	φCH
62			635	4.74	0.69	644	633	φCH
63	625		619	2.74	2.91	634	623	φCN
64	600		610	14.49	8.69	623	612	φCN
65	514		510	3.45	2.70	513	504	φCN
66			440	24.15	1.41	462	454	φCH
67		429	412	88.65	1.32	422	415	φCN
68			390	1.58	0.15	412	405	φCN
69		398	370	2.92	2.76	401	394	φCH
70			348	0.92	0.59	357	351	φNO
71		312	318	1.28	0.47	326	321	φCH
72			307	1.78	3.59	300	295	φCH
73			288	1.17	0.72	297	292	φCCC
74		223	206	0.26	1.31	210	206	φCCC
75		144	152	1.45	2.02	156	153	φCCN
76		102	123	1.01	3.00	122	120	φCCC
77		87	92	1.44	1.05	89	88	φCNC
78		76	81	1.43	1.44	78	77	φCNC
79			37	1.45	0.92	36	36	φCNC
80			30	0.87	2.02	28	27	φCCN
81			25	0.33	3.08	21	21	φCCN

γ: stretching; β: in-plane bending; φ: out-of-plane bending; I_{IR}: IR intensity; S_{Raman}: Raman scattering activity.

3.10.1. O–H vibrations

The OH group gives rise to three vibrations namely, stretching, in-plane bending and out-of-plane bending vibrations. They are likely to be the most sensitive to the environment, so they show pronounced shifts in the spectra of the hydrogen-bonded species. In case of un-substituted phenols, it has been shown that the frequency of OH stretching vibration in the gas phase appeared around 3657 cm^{-1} [32]. The H3IPI molecule manifested a weak band in its FT-IR spectrum at 3208 cm^{-1}, which was assigned to OH stretching vibration. A comparison of this band with the literature data predicted that there is a negative deviation of about 300 cm^{-1}. This might be due to inter-molecular hydrogen bonding. The in-plane and out-of-plane bending vibrations were observed at 1644 and 1230 cm^{-1}, respectively.

3.10.2. C-H vibrations

The aromatic derivatives give rise to C-H stretching, C-H in-plane and C-H out-of-plane bending vibrations. Aromatic compounds commonly exhibit multiple weak bands in the region 3100–3000 cm^{-1} [33] due to aromatic C-H stretching vibrations and they are not appreciably affected by the nature of the substituents [34]. The C–H vibrations of the title compound were observed as very weak bands at 3148, 3116, 3049 and 3002 cm^{-1} in its FT-IR spectrum and at 3148, 3063, 3022, 2974 and 2859 cm^{-1} in its FT-Raman spectrum. This mode was calculated in the range of 3038-3011 cm^{-1} with B3LYP/6-311++G(d,p) and in the range of 2934-3128 cm^{-1} with HF method. As expected, these modes (2-12 modes) are pure stretching modes as it is evident from the PED assignment column.

The bands due to C-H in-plane bending vibrations appeared in the region of 1000–1300 cm^{-1} [35]. The C-H in-plane bending vibrations of H3IPI were noted at 1277, 1255, 1184, 1105, 997 and 972 cm^{-1} in the FT-IR spectrum and at 1279, 1164, 1158, 998 and 924 cm^{-1} in its FT-Raman spectrum. The theoretically scaled vibrations by B3LYP/6-311++G(d,p) level method showed good agreement with experimentally recorded data.

The C-H out-of-plane bending vibrations usually occur within the region of 980-717 cm^{-1} [35]. This vibration mode was identified at 758, 699 and 672 cm^{-1} in the FT-IR spectrum of the H3IPI molecule and at 671, 654 and 398 in its FT-Raman spectrum.

3.10.3. Ring vibrations

The aromatic ring stretching vibrations are expected within the region of 1300-1000 cm^{-1} [36]. Most of the aromatic ring modes are altered by ring substitutions. The bands with different intensities were observed at 1600, 1574, 1507, 1351, 1313 and 1296 cm^{-1} in the FT-IR spectrum and at 1597, 1515, 1497 and 1344 cm^{-1} in the FT-Raman spectrum have been assigned to C-C stretching vibrations of the H3IPI molecule. All these vibrations appeared with mixed modes in the PED except three as evident by their strong intensities. The in-plane deformations were observed as expected at higher frequencies than the out-of-plane vibrations. The theoretical values exhibited excellent agreement with experimental ones.

3.10.4. C-N vibrations

The identification of C–N vibration bands is a very difficult task due to their overlapping with other several bands. Silverstein [37] assigned C–N stretching absorption in the region of 1382–1266 cm^{-1}. These vibration bands occurred at 1474, 1455 and 1441 cm^{-1} in the FT-IR spectrum of H3IPI and were observed at 1476 and 1400 cm^{-1} in its FT-Raman spectrum.

The C-N in-plane bending vibrations of H3IPI appeared at 1102 in its FT-Raman spectrum and at 1079 and 1040 cm^{-1} in its FT-IR spectrum. The theoretically scaled vibrations by B3LYP/6-311++G(d,p) level method also showed good agreement with experimentally recorded data.

The C-N out-of-plane bending vibrations usually appear within the region of 980-717 cm^{-1}. These vibrations were identified at 625, 600 and 514 cm^{-1} in FT-IR spectrum of H3IPI and at 429 cm^{-1} in its FT-Raman spectrum.

3.10.5. N-O vibrations

The characteristics group frequencies of the NO_2 group are independent on the rest of the molecule. In addition, wagging and twisting modes would be expected to be depolarized for out-of-plane vibrations. Aromatic nitro compounds have strong absorptions due to stretching vibrations of the NO_2 group at 1570-1485 cm^{-1} and 1370-1320 cm^{-1} [38]. The NO stretching mode of H3IPI was identified at 1368 in its FT-IR spectrum and at 1369 cm^{-1} in its FT-Raman spectrum. The in-plane bending modes of the NO group of H3IPI were assigned at 1024 and 1027 cm^{-1} in its FT-IR and FT-Raman spectra, respectively.

3.11. Error analysis of different vibrational calculations

The unscaled theoretical wavenumbers of the H3IPI molecule are overestimated and hence were scaled by different scaling factors. This is quite obvious, since the calculated frequencies are harmonic in nature, whereas the experimental frequencies may involve anharmonicity. In order to reduce the standard deviation between the unscaled and observed fundamentals, overall scale factors were used. A close agreement between the experimental and scaled wavenumbers is mostly achieved in the fingerprint region. Both HF and DFT (B3LYP) methods showed a uniform deviation after scaling, but the HF method manifested more deviation than the DFT (B3LYP) method. The correlation between the calculated and experimental frequencies using both HF and DFT (B3LYP) methods are linear (Figure S3) and is described by the following equations:

B3LYP

$$\partial cal = -19.03218 + 1.02191\,\partial exp \qquad (R^2 = 0.99598) \tag{12}$$

HF

$$\partial cal = -17.1797 + 1.02827\ \partial \exp \qquad (R^2 = 0.99310) \qquad (13)$$

Therefore, the calculated frequencies by B3LYP/6-311++G(d,p) method seem to be more closer to the experimental values than that calculated by the HF method.

4. Conclusions

The title compound H3IPI is an oxime-bearing precursor to potential antifungal agents and has been thoroughly characterized with various spectroscopic tools. Perfect normal co-ordinates of the title molecule were performed using DFT-B3LYP and HF methods with 6-311++G(d,p) basis set. The calculated frequencies of H3IPI by B3LYP/6-311++G(d,p) method is good fitted with the experimental values. The experimental X-ray diffraction data are quite close to the optimized values. The calculated bond angles values of H3IPI suggest that the ring of the molecule is deformed which might be due to steric and electronic factors. All hydrogen atoms of H3IPI manifested positive natural charges which are greater in values than their corresponding Mulliken charges. The correlation equations between heat capacities, entropies, enthalpy changes and temperatures are represented by quadratic polynomial formulas. The energy break of HOMO–LUMO of H3IPI explains the charge shift interactions within the molecule, which influences its biological activity. The calculated dipole moment and first hyperpolarizability of the title molecule are 1.32 and 3.66 times, respectively, as that of urea which gives the possibility to be a new NLO compound. The molecular orbital coefficient studies of H3IPI proposed that its electronic spectrum corresponds to the $\pi \rightarrow \pi^*$ electronic transition. The NBO analysis has been executed for the title compound at the B3LYP/6-311++G(d,p) level in order to clarify the intramolecular, re-hybridization and delocalization of electron density within the molecule. The performance of the B3LYP method with respect to the prediction of the NMR chemical shifts within the H3IPI molecule is in a good agreement with the experimental values. The current comprehensive spectroscopic characterization of H3IPI and the computations thereof could support pharmacomodulation of the title compound to develop new potent antifungal candidates.

Acknowledgment: The authors would like to extend their sincere appreciation to the Deanship of Scientific Research at King Saud University for its funding of this research through the Research Group Project No. RG-1438-083.

References

[1] D. Enoch, H. Ludlam, N. Brown, Invasive fungal infections: a review of epidemiology and management options, J. Med. Microbiol. 55 (7) (2006) 809–818.

[2] G.D. Brown, D.W. Denning, S.M. Levitz, Tackling human fungal infections, Science 336 (6082) (2012) 647–647.

[3] B.J. Park, K.A. Wannemuehler, B.J. Marston, N. Govender, P.G. Pappas, T.M. Chiller, Estimation of the current global burden of cryptococcal meningitis among persons living with HIV/AIDS, Aids 23 (4) (2009) 525–530.

[4] S. Arikan, J. Rex, Nystatin LF (Aronex/Abbott), Current opinion in investigational drugs (London, England: 2000) 2 (4) (2001) 488–495.

[5] D.W. Denning, Echinocandin antifungal drugs, The Lancet 362 (9390) (2003) 1142–1151.

[6] V. Moudgal, J. Sobel, Antifungals to treat Candida albicans, Expert Opin. Pharmacother. 11 (12) (2010) 2037–2048.

[7] J. Heeres, L. Meerpoel, P. Lewi, Conazoles, Molecules 15 (6) (2010) 4129–4188.

[8] G.M. Eliopoulos, S. Perea, T.F. Patterson, Antifungal resistance in pathogenic fungi, Clin. Infect. Dis. 35 (9) (2002) 1073–1080.

[9] S. Mishra, P. Singh, Hybrid molecules: The privileged scaffolds for various pharmaceuticals, Eur. J. Med. Chem. 124 (2016) 500–536.

[10] M.N. Aboul-Enein, A.A.E.S. El-Azzouny, M.I. Attia, O.A. Saleh, A.L. Kansoh, Synthesis and anti-*Candida* potential of certain novel 1-[(3-substituted-3-phenyl) propyl]-1*H*-imidazoles, Archiv der Pharm. 344 (12) (2011) 794–801.

[11] G. Roman, M. Mareş, V. Năstasă, A novel antifungal agent with broad spectrum: 1-(4-biphenylyl)-3-(1*H*-imidazol-1-yl)-1-propanone, Archiv der Pharm. 346 (2) (2013) 110–118.

[12] M.I. Attia, A.A. Radwan, A.S. Zakaria, M.S. Almutairi, S.W. Ghoneim, 1-Aryl-3-(1 *H*-imidazol-1-yl)propan-1-ol esters: synthesis, anti-*Candida* potential and molecular modeling studies, Chem. Cent. J. 7 (1) (2013) 168.

[13] M.I. Attia, A.S. Zakaria, M.S. Almutairi, S.W. Ghoneim, In vitro anti-*Candida* activity of certain new 3-(1*H*-imidazol-1-yl)propan-1-one oxime esters, Molecules 18 (10) (2013) 12208–12221.

[14] A. Rossello, S. Bertini, A. Lapucci, M. Macchia, A. Martinelli, S. Rapposelli, E. Herreros, B. Macchia, Synthesis, antifungal activity, and molecular modeling studies of new inverted oxime ethers of oxiconazole, J. Med. Chem. 45 (22) (2002) 4903–4912.

[15] L.F. Tietze, H.P. Bell, S. Chandrasekhar, Natural product hybrids as new leads for drug discovery, Angew. Chem. Int. Ed. 42 (34) (2003) 3996–4028.

[16] M. Frisch, G. Trucks, H. Schlegel, G. Scuseria, M. Robb, J. Cheeseman, J. Montgomery Jr, T. Vreven, K. Kudin, J. Burant, Gaussian 03, revision c. 02; Gaussian, Inc., Wallingford, CT 4 (2004).

[17] D.C. Young, A Practical Guide for Applying Techniques to Real-World Problems, Wiley–Interscience New York:, 2001.

[18] M. Karabacak, A. Çoruh, M. Kurt, FT-IR, FT-Raman, NMR spectra, and molecular structure investigation of 2, 3-dibromo-N-methylmaleimide: A combined experimental and theoretical study, J. Mol. Struct. 892 (1-3) (2008) 125–131.

[19] N. Sundaraganesan, S. Ilakiamani, H. Saleem, P.M. Wojciechowski, D. Michalska, FT-Raman and FT-IR spectra, vibrational assignments and density functional studies of 5-bromo-2-nitropyridine, Spectrochim. Acta A: Mol. Biomol. Spectrosc. 61 (13-14) (2005) 2995–3001.

[20] M.H. Jamróz, Vibrational energy distribution analysis (VEDA): scopes and limitations, Spectrochim. Acta A: Mol. Biomol. Spectrosc. 114 (2013) 220–230.

[21] R. Dennington, T. Keith, J. Millam, K. Eppinnett, W.L. Hovell, R. Gilliland, GaussView, Version, 2009.

[22] P.S. Peek, D.P. McDermott, Vibrational modes and frequencies of 2-pyrrolidinones and their deutero-isotopomers, Spectrochim. Acta A: Mol. Biomol. Spectrosc. 44 (4) (1988) 371–377.

[23] H.-K. Fun, C.K. Quah, M.I. Attia, M.S. Almutairi, S.W. Ghoneim, (*E*)-*N*-[3-(Imidazol-1-yl)-1-phenylpropylidene]hydroxylamine, Acta Cryst. E 68 (3) (2012) o627–o627.

[24] J.B. Ott, J. Boerio-Goates, Calculations from statistical thermodynamics, Academic Press, 2000.

[25] R. Zhang, B. Du, G. Sun, Y. Sun, Experimental and theoretical studies on o-, m- and p-chlorobenzylideneaminoantipyrines, Spectrochim. Acta A: Mol. Biomol. Spectrosc. 75 (3) (2010) 1115–1124.

[26] I. Fleming, Frontier orbitals and organic chemical reactions, Wiley1977.

[27] N.M. O'boyle, A.L. Tenderholt, K.M. Langner, Cclib: a library for package-independent computational chemistry algorithms, J. Comput. Chem. 29 (5) (2008) 839–845.

[28] S. Murray, K. Sen, Molecular electrostatic potentials: concepts and applications, Elsevier1996.

[29] J. Šponer, P. Hobza, DNA base amino groups and their role in molecular interactions: Ab initio and preliminary density functional theory calculations, Int. J. Quantum Chem. 57 (5) (1996) 959–970.

[30] G. Fogarasi, X. Zhou, P.W. Taylor, P. Pulay, The calculation of ab initio molecular geometries: efficient optimization by natural internal coordinates and empirical correction by offset forces, J. Am. Chem. Soc. 114 (21) (1992) 8191–8201.

[31] G. Socrates, Infrared and Raman characteristic group frequencies: tables and charts, John Wiley & Sons2001.

[32] N. Sundaraganesan, B. Anand, B.D. Joshua, Vibrational spectroscopy investigation using ab initio and density functional theory analysis on the structure of 2-amino-5-methylphenol, Spectrochim. Acta A: Mol. Biomol. Spectrosc. 67 (2) (2007) 550–558.

[33] V. Krishnakumar, R.J. Xavier, Normal coordinate analysis of 2-mercapto and 4,6-dihydroxy-2-mercapto pyrimidines, Indian J. Pure & Appl. Phys. 41 (2003) 597–601.

[34] N. Colthup, Introduction to infrared and Raman spectroscopy, Elsevier 2012.

[35] A. Srivastava, V. Singh, Theoretical and experimental studies of vibrational spectra of naphthalene and its cation, Indian J. Pure & Appl. Phys. 45 (2007) 714–720.

[36] D. Lin-Vien, N.B. Colthup, W.G. Fateley, J.G. Grasselli, The handbook of infrared and Raman characteristic frequencies of organic molecules, Elsevier 1991.

[37] R.M. Silverstein, G.C. Bassler, Spectrometric identification of organic compounds, J. Chem. Educ. 39 (11) (1962) 546.

[38] R. Shunmugam, D. Sathyanarayana, Raman and polarized infrared spectra of pyridine-2-thione, Spectrochim. Acta A: Mol. Biomol. Spectrosc. 40 (8) (1984) 757–761.

Figures captions

Figure 1: Theoretical optimized geometric structure with atoms numbering of H3IPI.

Figure 2: The scan picture of the H3IPI molecule.

Figure 3: The Mulliken and natural charge distribution of the H3IPI molecule.

Figure 4: Correlation graph of heat capacity, entropy, enthalpy and temperature for H3IPI.

Figure 5: Molecular orbitals and energies for the HOMO and LUMO of H3IPI.

Figure 6: Molecular electrostatic potential (MEP and ED) map in the gas phase of H3IPI.

Figure 7: Experimental and simulated Infrared spectra of H3IPI.

Figure 8: Experimental and simulated Raman spectra of H3IPI.

Scheme 1: Synthesis of the title compound **3**.

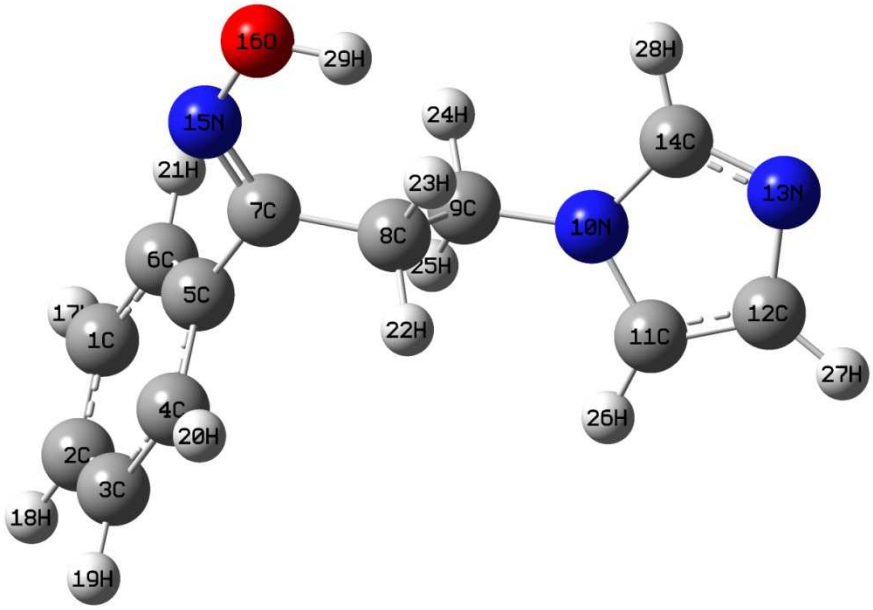

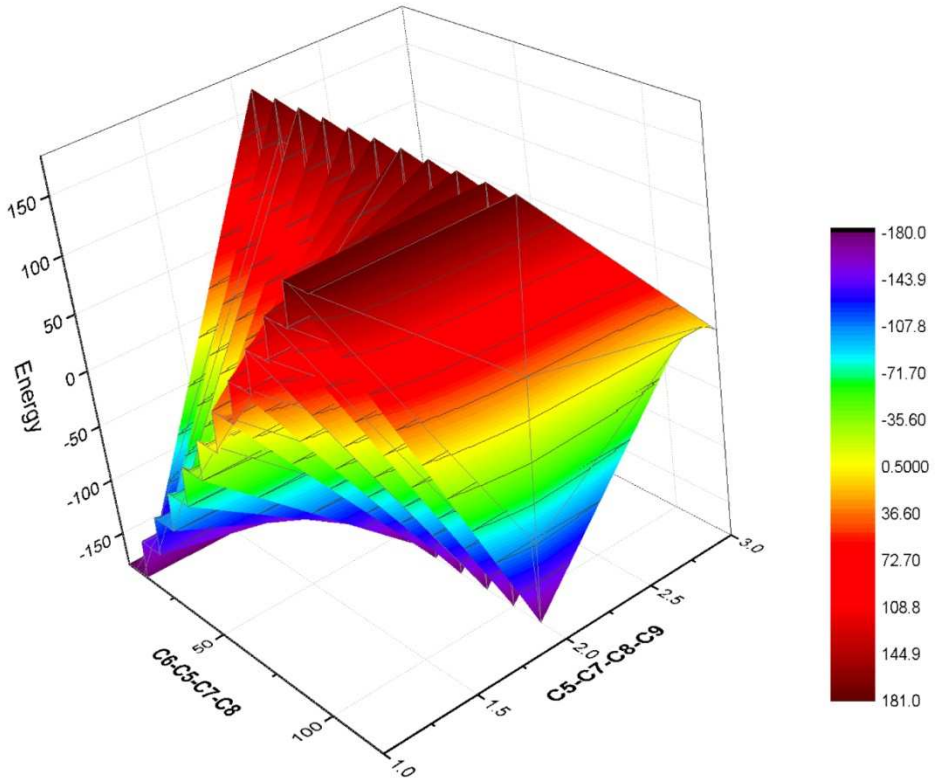

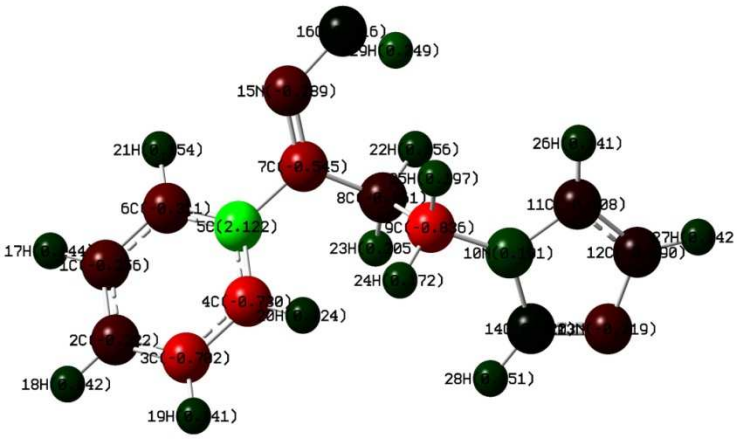

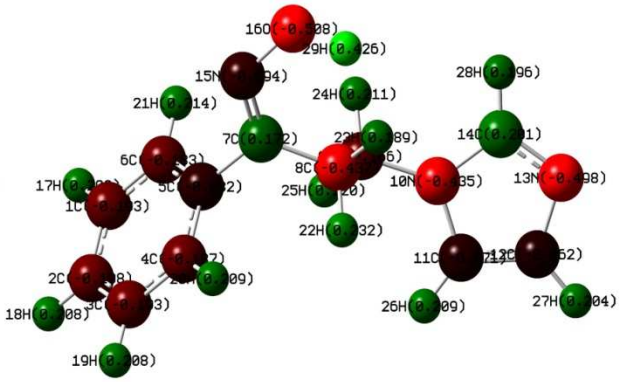

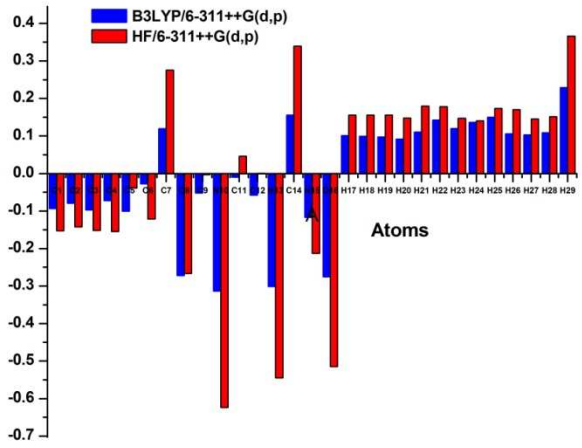

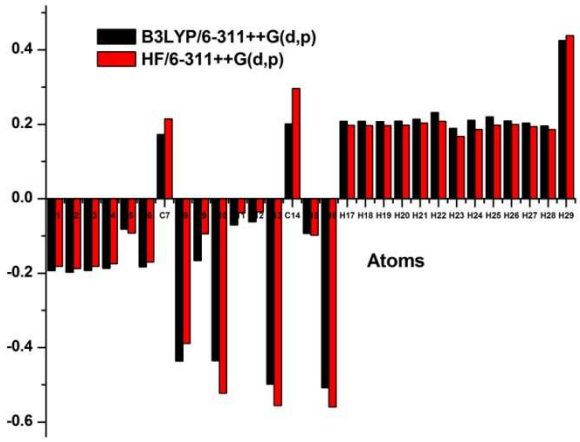

Muillken charge distribution

Natural charge distribution

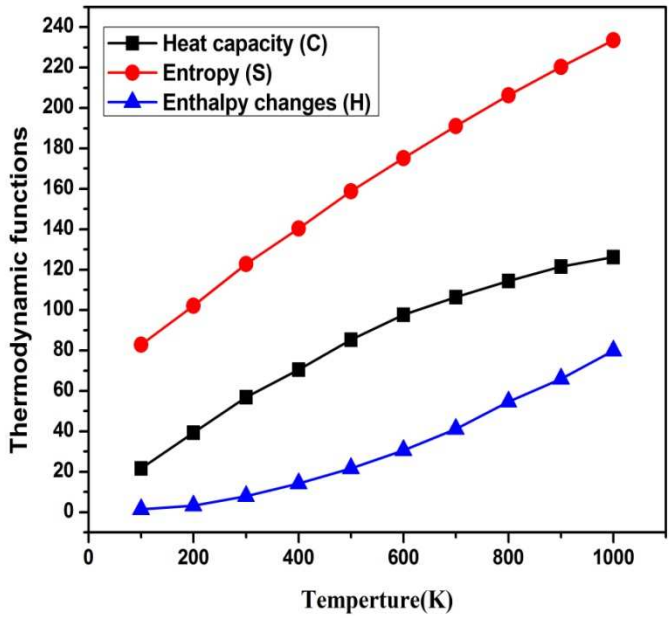

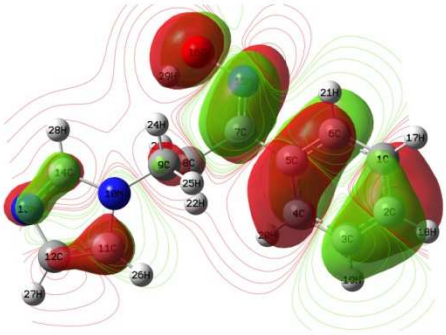

HOMO - 1 = -6.7090

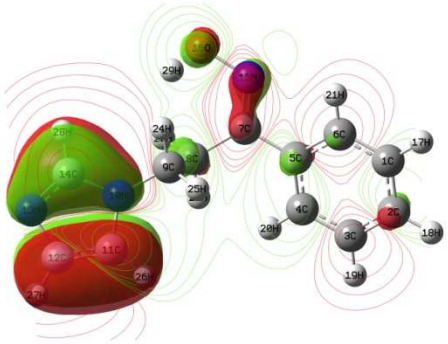

HOMO = -6.5065

HOMO - 1 - LUMO +1 = -6.0474

HOMO - LUMO = -4.9518

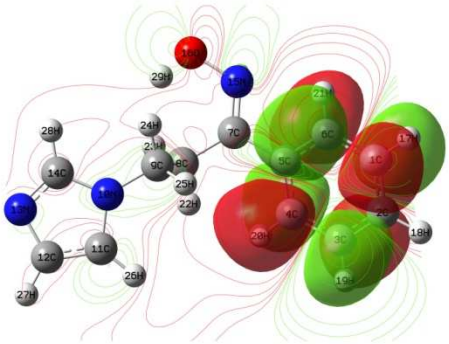

LUMO + 1 = -0.6615

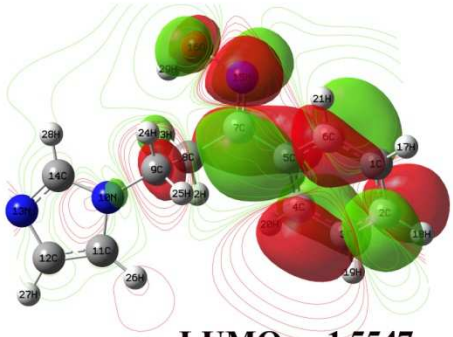

LUMO = -1.5547

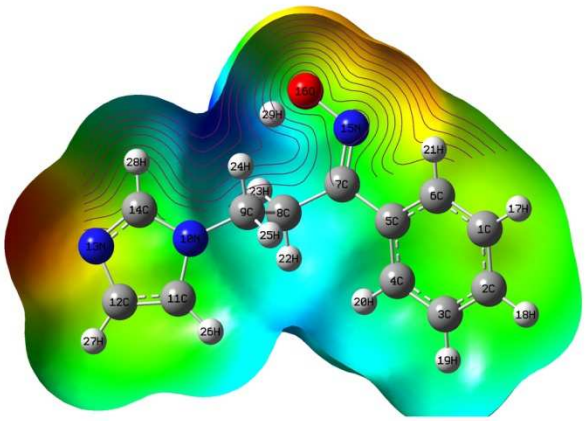

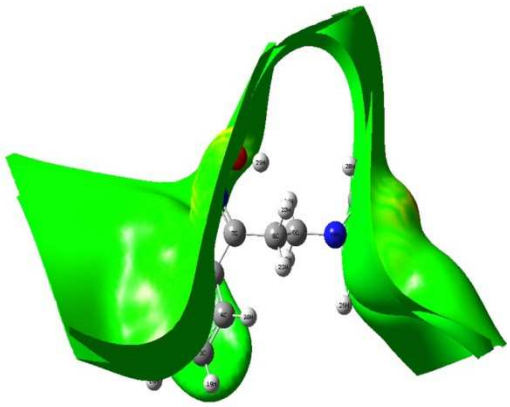

-0.01766 to +0.01766

-0.05929 to +0.05929

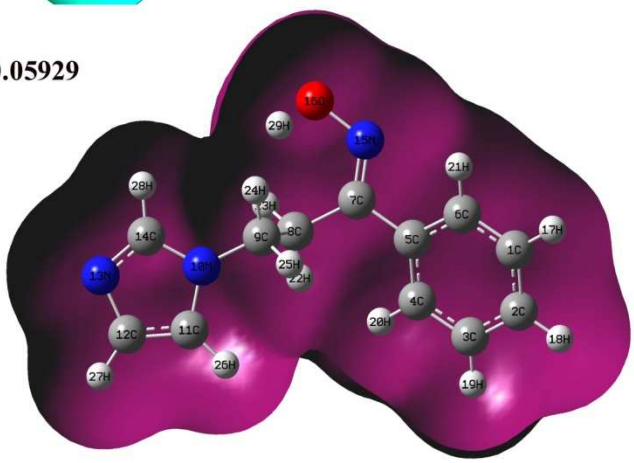

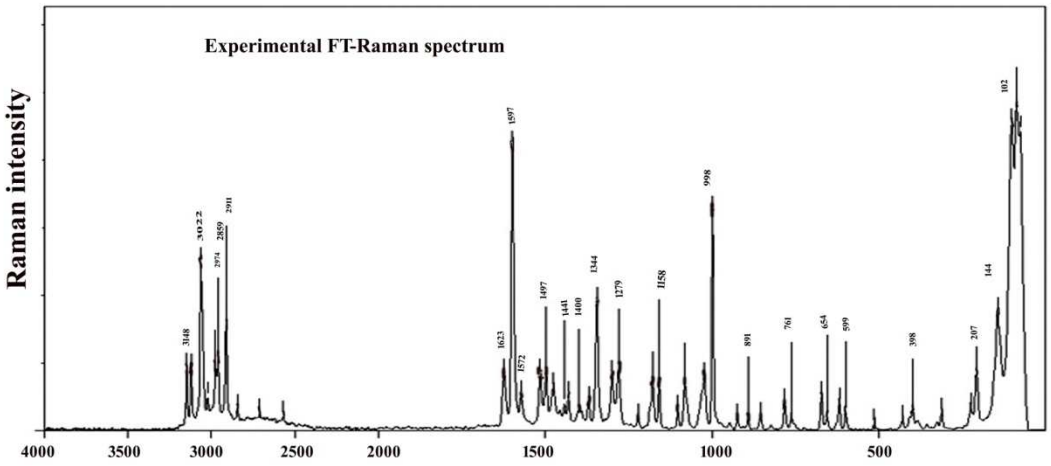

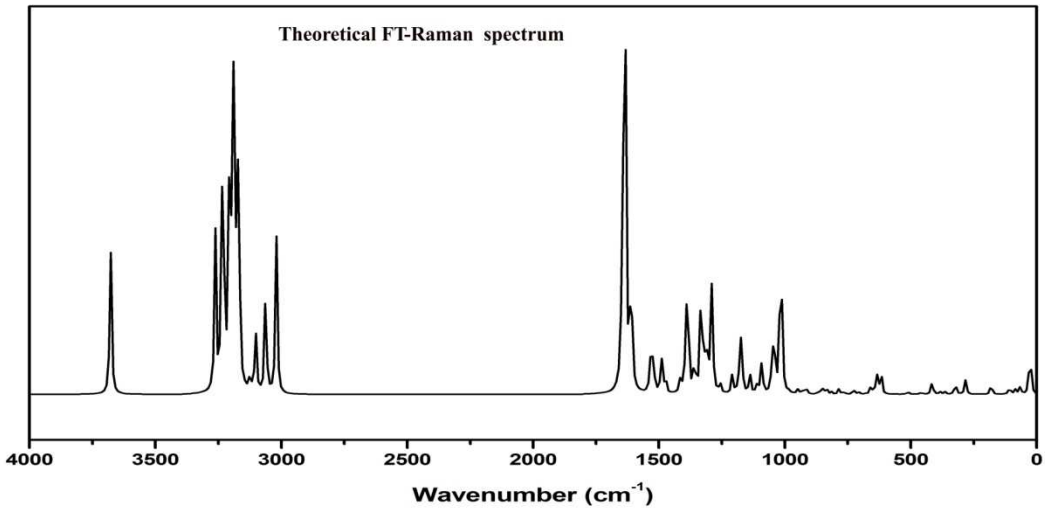

.

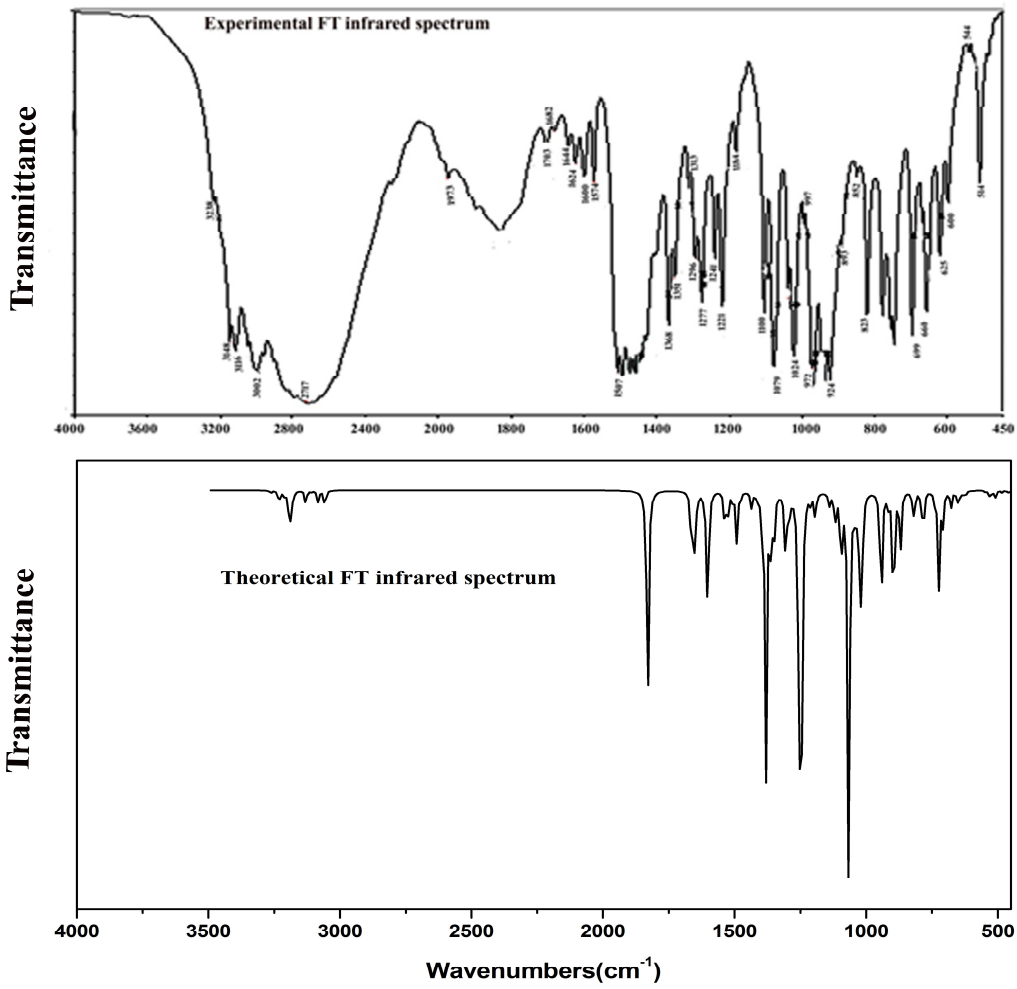
Experimental FT infrared spectrum
Transmittance
4000
3600
3200
2800
2400
2000
1800
1600
1400
1200
1000
800
600
450
Theoretical FT infrared spectrum
Transmittance
4000
3500
3000
2500
2000
1500
1000
500
Wavenumbers(cm-1)

- Spectroscopic analysis of an oxime, a precursor to potential antifungal agents.
- FT-IR, FT-Raman, ^{1}H and ^{13}C NMR spectral analyses were recorded.
- The geometrical parameters are in good agreement with XRD data.
- The HOMO-LUMO and NLO properties of the title molecule were studied.